
This is an electronic reprint of the original article.
This reprint may differ from the original in pagination and typographic detail.

de Guzman, Mar Francis; Hassan, Muhammad; Haneda, Katsuyuki
Uncertainty of millimeter-wave channel sounder due to integration of frequency converters

Published in:
2021 17th International Symposium on Wireless Communication Systems, ISWCS 2021

DOI:
[10.1109/ISWCS49558.2021.9562208](https://doi.org/10.1109/ISWCS49558.2021.9562208)

Published: 06/09/2021

Document Version
Peer-reviewed accepted author manuscript, also known as Final accepted manuscript or Post-print

Please cite the original version:
de Guzman, M. F., Hassan, M., & Haneda, K. (2021). Uncertainty of millimeter-wave channel sounder due to integration of frequency converters. In *2021 17th International Symposium on Wireless Communication Systems, ISWCS 2021* (Vol. 2021-September). (International Symposium on Wireless Communication Systems). IEEE. <https://doi.org/10.1109/ISWCS49558.2021.9562208>

This material is protected by copyright and other intellectual property rights, and duplication or sale of all or part of any of the repository collections is not permitted, except that material may be duplicated by you for your research use or educational purposes in electronic or print form. You must obtain permission for any other use. Electronic or print copies may not be offered, whether for sale or otherwise to anyone who is not an authorised user.

This is an electronic reprint of the original article.
This reprint may differ from the original in pagination and typographic detail.

De Guzman, Mar Francis; Hassan, Muhammad; Haneda, Katsuyuki

Uncertainty of Millimeter-Wave Channel Sounder due to Integration of Frequency Converters

Published in:
2021 17th International Symposium on Wireless Communication Systems (ISWCS)

DOI: [10.1109/ISWCS49558.2021.9562208](https://doi.org/10.1109/ISWCS49558.2021.9562208)

Published: 06/09/2021

Document Version
Peer reviewed version

Please cite the original version:
M. F. De Guzman, M. Hassan and K. Haneda, "Uncertainty of Millimeter-Wave Channel Sounder due to Integration of Frequency Converters," 2021 17th International Symposium on Wireless Communication Systems (ISWCS), 2021, pp. 1-6, doi: [10.1109/ISWCS49558.2021.9562208](https://doi.org/10.1109/ISWCS49558.2021.9562208).

This material is protected by copyright and other intellectual property rights, and duplication or sale of all or part of any of the repository collections is not permitted, except that material may be duplicated by you for your research use or educational purposes in electronic or print form. You must obtain permission for any other use. Electronic or print copies may not be offered, whether for sale or otherwise to anyone who is not an authorised user.

Uncertainty of Millimeter-Wave Channel Sounder due to Integration of Frequency Converters

Mar Francis De Guzman^{1,2}, Muhammad Hassan¹ and Katsuyuki Haneda¹

¹ Aalto University School of Electrical Engineering, Espoo, Finland E-mail: francis.deguzman@aalto.fi

² Advanced Science and Technology Institute, Department of Science and Technology, Quezon City, Philippines

Abstract—In this study, we investigate the possible sources of measurement uncertainties with the integration of radio over fiber solution and frequency converters in millimeter-wave sounders. We examined analytically the effect of phase variations due to the disturbance of the optical fiber cable, the limited sideband suppression of the frequency converters, and the influence of the dispersion in rectangular waveguides to the response of the channel sounder. Characterization of the optical fiber cable confirms that disturbance of the cable leads only to phase variation. Back-to-back measurements of Aalto’s sounder operating at V- and D-bands also verify that disturbance of the cable supplying the local (LO) continuous-wave signals are most influential to the stability of frequency- and delay-domain responses of the sounder because the LO signals undergo frequency multiplication. We found that the V-band and D-band channel sounders, with at least 17 dB and 20 dB Image Rejection Ratio, have the maximum gain variation of 0.5 dB and 1.0 dB in the peak of channel impulse responses when subject to different fiber cable positions.

I. INTRODUCTION

Cellular radios for the current and future generations, i.e., fifth-generation and beyond, will exploit higher frequencies than legacy band of 3.5 GHz actively to leverage wider bandwidth. Radio channel sounding is an essential activity in developing a channel model that is used for benchmarking novel physical layer schemes against the legacy. Radio channel sounding at the interested frequency band is therefore an essential activity, typically at millimetre-wave (mm-wave) bands in the present case. Usually mm-wave channel sounding is performed by integrating external microwave circuits with conventional radio channel sounder operating at the legacy band. Baseband or intermediate frequency (IF) signals generated by the conventional channel sounder is frequency-converted to mm-wave radio frequency (RF) bands, e.g., [1] and references therein. The microwave circuits for mm-wave frequency conversion can be off-the-shelf components such as mixers, frequency multipliers and filters.

Uncertainty of channel sounding is influenced by every component in the sounder, including instruments, digital signal processing methods and microwave components. Calibration of a sounder is essential in reducing the uncertainty of the hardware. It is accomplished through back-to-back (B2B) calibration, e.g., [2] and antenna array calibration, e.g., [3]. The former measures transfer functions and often performs power sweeps of the sounder hardware by bypassing antennas, allowing us to remove the linear or non-linear sounder transfer function from radio channel measurements. While the latter

aims at compensating for non-ideal responses of antenna arrays mainly due to mutual coupling, which is important for accurate directional characterization of radio channels.

It is usually assumed that hardware states during calibration measurements remain the same throughout the subsequent field measurements for radio channels where the calibration is applied to compensate for the hardware states. In practice, however, it is almost inevitable to avoid changing state of the hardware due to various reasons, e.g., changes in surrounding temperature, mechanical stress on cables and sensitivity of sounder hardware responses to those changes. It is clear that the sounder hardware and architecture should be designed so that it is robust to those external changes during measurements.

The present paper illustrates an example of uncertainties of an mm-wave channel sounder due to different sounder components, e.g., radio-over-fiber cables, off-the-shelf frequency converters and waveguides. We show that phase variations due to physical stress on cables carrying the IF and local oscillator (LO) signals can lead to noticeable *magnitude* fluctuation of the sounder transfer function, unless off-the-shelf converters are properly interfaced with legacy channel sounder providing baseband or IF signals. We discuss the improper sideband reduction at frequency converters as an example of the interfacing issue. We also demonstrate the uncertainties using Aalto’s mm-wave channel sounder, illustrated in Fig. 1, that integrates a vector network analyzer (VNA) and frequency converters. The VNA provides IF signal of channel sounding while two sets of frequency converters are introduced to perform sounding at V- and D-bands [4], [5].

To summarize, two problems the present paper addresses are

- *Impacts of interfacing between radio components* on overall mm-wave sounder operation when integrating off-the-shelf frequency converters and a legacy sounder operating at the baseband or IF; and
- *Impacts of uncertainty in each radio component*, which is subject to possible changes of the surrounding environmental conditions, on overall mm-wave sounder operation.

The two main contributions of this work are

- *Mathematical formulations* that relate sources of uncertainty in radio components of an mm-wave channel sounder with its overall responses; and

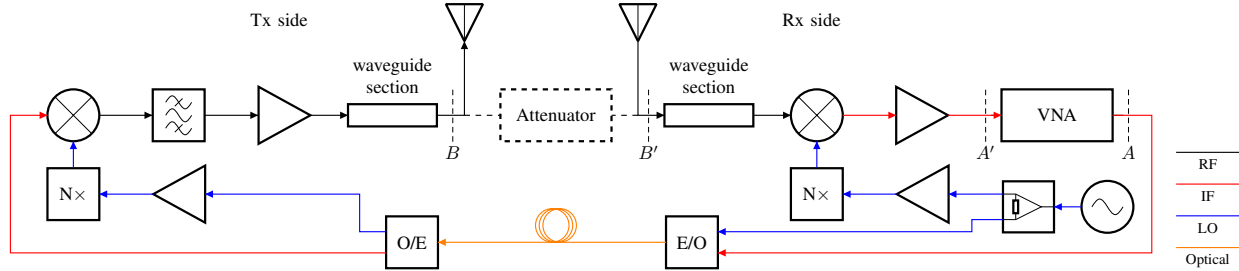


Fig. 1. Aalto's mm-wave channel sounder.

- *Experimental evidence* that demonstrates impacts of interfacing between legacy channel sounder and frequency converters on realized uncertainty of the mm-wave channel sounder.

The remainder of this paper is organized as follows. Section II introduces channel sounder along with its back-to-back calibration. Section III provides a mathematical model of uncertainty in channel sounder's response due to perturbation to hardware, i.e., optical fiber cable in the present case. Section IV describes experimental set-up of our mm-wave channel sounder to demonstrate the effects of the fiber cable on responses of the sounder and to verify the mathematical model. The paper is concluded in Section V.

II. VNA-BASED CHANNEL SOUNDER

A. Architecture

An architecture of Aalto's mm-wave channel sounder is shown in Fig. 1. It is a frequency-domain measurement system that uses VNA to achieve wider bandwidth and high dynamic range which translate to finer temporal resolution and highly sensitive or long-range measurements. Frequency converters are integrated to translate the IF from the VNA to mm-wave RF bands. The converters are injected with LO signal from a single continuous-wave source on the Rx side. The LO signals are subject to frequency multipliers, which have multiply factor N , before mixed with the IF signals. Hence, the upper sideband RF f_{rf} is related to the IF f_{if} and LO signal frequency f_{lo} as $f_{rf} = Nf_{lo} + f_{if}$. A 10 MHz signal from the VNA is used to synchronize the LO source and the VNA. To minimize signal loss and enable long-range sounding, a Radio over Fiber (RoF) solution consisting of Optical-to-Electrical (O/E) and Electrical-to-Optical (E/O) converters, and a military-grade optical fiber cable having two single-mode fibers is employed so that the IF and LO signals can be shared to the Tx side. As the IF signal input to the frequency upconverter is supplied from the VNA, a single-sideband RF channel is realized by suppressing the image signal generated in the mixer in two ways, e.g., 1) by inserting a hybrid coupler to create in-band (I) or quadrature (Q) components when the mixer accepts I/Q inputs and 2) by appending a bandpass filter (BPF) at the RF port of the mixer, or 3) combination of 1) and 2). In practice, mm-wave frequency converter modules from vendors

have different inputs; some accept I/Q input with a built-in RF bandpass filter, while some other have only one of I or Q inputs without a built-in RF filter.

B. Back-to-back Calibration Measurements

The VNA performs frequency sweep and producing the forward transmission scattering parameter $S_{A'A}$. It is approximately equal to the complex transfer function $H(f)$ where f is a frequency of signals at the equivalent baseband, of the system seen between the reference planes A and A' as shown in Fig. 1. We also define here the channel sounder transfer function as $H_{cs}(f) = S_{BA} \cdot S_{A'B'}$. Since the VNA also measures the $H_{cs}(f)$, B2B calibration must be performed. B2B calibration is an essential step in reducing the systematic errors caused by the hardware components of the sounder. An example of such errors is the spurious peak in the CIR resulting from signal reflections within the sounder's components [6]. These spurs may result in misvaluation of the channel characteristics if not reduced through proper calibration.

In our case, B2B measurement is performed by removing the antennas and connecting an attenuator, with response of $H_{att}(f)$, between the transmitter and receiver in Fig. 1. The transfer function from the B2B measurement is

$$H_{b2b}(f) = H_{cs}(f) \cdot H_{att}(f). \quad (1)$$

The transfer function obtained at the VNA when performing channel measurements is given by

$$H(f) = H_{cs}(f) \cdot H_{dut}(f), \quad (2)$$

where $H_{dut}(f)$ is the transfer function of the device-under-test (DUT) between the reference planes B and B' . In our case, the DUT is the radio channel that we want to characterize. The DUT transfer function $H_{dut}(f)$ can be solved by using Eq. (1) and (2) as

$$H_{dut}(f) = \frac{H(f)}{H_{cs}(f)} = H(f) \cdot \frac{H_{att}(f)}{H_{b2b}(f)}. \quad (3)$$

Note that $H_{dut}(f)$ includes the effects of the antennas and additional waveguide sections which must also be accounted for when extracting the over-the-air (OTA) radio channel transfer function. Finally, the channel impulse response (CIR) $h(\tau)$, where τ is the delay, can be calculated by performing inverse fast Fourier transform (IFFT) of the transfer function.

III. MEASUREMENT UNCERTAINTIES

To acquire a precise estimate of $H_{\text{dut}}(f)$, it is desired that the $H_{\text{cs}}(f)$ remain constant during B2B and OTA measurements. However, measurement campaigns are usually lengthy and typically take hours or even days, during which sounder's hardware components are subject to temperature variation and different physical stresses. Therefore estimated $H_{\text{cs}}(f)$ at the beginning of the measurement campaign may become outdated and lead to errors of estimated $H_{\text{dut}}(f)$ by (3). We can then express the measured transfer function in Eq. (2) to incorporate these changes as

$$H(f) = \Delta H_{\text{cs}}(f) \cdot H_{\text{cs}}(f) \cdot H_{\text{dut}}(f), \quad (4)$$

where $\Delta H_{\text{cs}}(f)$ is the change in channel sounder transfer function. The magnitude and phase components of this change are denoted here as $\Delta|H_{\text{cs}}(f)|$ and $\Delta\psi$, respectively. In this section, we analyze the extent of outdated estimates of $H_{\text{dut}}(f)$ due to channel sounder components.

A. Characterization of Optical Fiber Cable Effects

One of the components that is sensitive to external disturbance is the optical fiber cable that can cause signal phase variations [7]. To understand the impact of these phase changes in fiber cable on $H_{\text{cs}}(f)$, an equivalent signal block diagram of the sounder in B2B configuration is elaborated in Fig. 2. Note that the transfer functions of the channel sounder components are assumed stable except for the fiber cable. Only the additional phase in IF and LO signals due to environmental disturbance to the fiber cable are incorporated in the diagram. They are represented as phase shift blocks $\phi(f)$ and θ , respectively. As the LO is a single continuous-wave tone, it is not necessary to look at the frequency dependency of θ . A BPF is added after the downconverter block to represent the inherent IF filtering process in the VNA. Furthermore, it is assumed that the RF BPF has limited rejection capability which results in a residual image signal with amplitude b compared to the level of the intended sideband. The amplitude b is more commonly termed Image Rejection Ratio (IRR) as a power ratio between desired and image signals and expressed as $IRR = 20 \cdot \log_{10}(1/b)$. Following this signal block diagram, the sounder transfer function can be associated to these phase shifts as

$$H_{\text{cs}}(f) = \frac{1}{4}e^{j\phi(f)}e^{-jN\theta} + \frac{b}{4}e^{j\phi(f)}e^{jN\theta}, \quad (5)$$

where the first term is the intended upper sideband (USB) component and the second term is the image lower sideband (LSB) component in this paper. The remaining image interferes with the intended sideband upon downconversion. The change in magnitude of $H_{\text{cs}}(f)$ can now be expressed as

$$\Delta|H_{\text{cs}}(f)| = |1 + be^{j2N\theta}|, \quad (6)$$

which shows its dependency on the phase disturbance θ on the LO signal path of the fiber cable. The phase disturbance influences the $\Delta|H_{\text{cs}}(f)|$, i.e. the magnitude is maximum when $e^{j2N\theta} = 1$ and minimum when $e^{j2N\theta} = -1$. In this

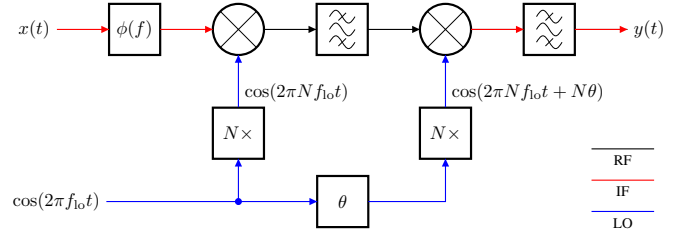


Fig. 2. Signal block diagram of the mmwave channel sounder in back-to-back configuration.

paper, we associate the measurement uncertainty with the minimum magnitude. Hence, the largest possible uncertainty in $|H_{\text{cs}}(f)|$ in dB due to limited sideband suppression is given by

$$U = 20 \cdot \log_{10} \left(\frac{1}{1-b} \right). \quad (7)$$

The amount of uncertainty can approach $+\infty$ dB when b approaches 1, i.e., no reduction of the image side band, and 0 dB when $b = 0$ in the case of total image suppression. Equation (7) also implies that at least 25 dB of IRR ($b = 0.0562$) is needed to achieve maximum uncertainty of 0.5 dB.

B. Frequency-dependent Uncertainty

The uncertainty U should also appear in CIR as is, provided that the only source of phase offset between the desired signal and the image signal is the phase disturbance θ . However, there is another phase offset due to the use of waveguides. Electromagnetic waves experience dispersion in waveguides leading to additional frequency-dependent phase offset. In particular, the group delay in rectangular waveguides with TE₁₀ mode of propagation, derived from Table 3.2 in [8], is given by

$$\tau_g(f_{\text{rf}}) = \frac{l}{c \cdot \sqrt{1 - \left(\frac{c}{2a \cdot f_{\text{rf}}} \right)^2}}, \quad (8)$$

where f_{rf} is in [Hz], l is the length of the waveguide [m], c is the speed of light [m/s], and a is the waveguide width [m]. This group delay can be linearized as $\tau'_g(f_{\text{rf}}) = \beta_1 \cdot f + \beta_0$ so that the group delay for the USB τ_u and LSB τ_l can be expressed as

$$\tau_u = \beta_1(Nf_{\text{lo}} + f_{\text{if}}) + \beta_0 = \tau_a + \tau_b, \quad (9)$$

$$\tau_l = \beta_1(Nf_{\text{lo}} - f_{\text{if}}) + \beta_0 = \tau_a - \tau_b, \quad (10)$$

where β_1 is the slope of the fitted line, β_0 is the y -intercept, $\tau_a = \beta_1 \cdot f_{\text{lo}} + \beta_0$ and $\tau_b = \beta_1 \cdot f_{\text{if}}$. The USB delay τ_u and LSB delay τ_l are included in (5) as

$$H_{\text{cs}}(f) = \frac{1}{4}e^{j\phi(f)}e^{-jN\theta}e^{-j2\pi(f_{\text{if}}+Nf_{\text{lo}})\tau_u} + \frac{b}{4}e^{j\phi(f)}e^{jN\theta}e^{-j2\pi(f_{\text{if}}-Nf_{\text{lo}})\tau_l}, \quad (11)$$

TABLE I
MEASUREMENT PARAMETERS

Parameter	V-band	D-band
f_{if} (GHz)	1 – 5	1.52 – 5.52
f_{lo} (GHz)	14.5	11.54
f_{if} (GHz)	59 – 63	140 – 144
N	4	12

which is further elaborated by using (9) and (10) as,

$$H_{cs}(f) = \frac{1}{4} e^{j\phi(f)} e^{-jN\theta} e^{-j2\pi(f_{if}\tau_a + Nf_{lo}\tau_b)} e^{-j2\pi(f_{if}\tau_b + Nf_{lo}\tau_a)} + \frac{b}{4} e^{j\phi(f)} e^{jN\theta} e^{-j2\pi(f_{if}\tau_a + Nf_{lo}\tau_b)} e^{j2\pi(f_{if}\tau_b + Nf_{lo}\tau_a)}. \quad (12)$$

A complete expression of $\Delta|H_{cs}(f)|$ considering the phase disturbances in the RoF and dispersion in the waveguide section can now be written as

$$\Delta|H_{cs}(f)| = \left| 1 + b e^{j2N\theta} e^{j4\pi(\beta_1 f_{if}^2 + \beta_0 N f_{lo}^2)} \right|, \quad (13)$$

which shows that $\Delta|H_{cs}(f)|$ depends not only with the phase disturbance θ , but also with f_{if}^2 .

C. Channel Impulse Response Distortion

In addition to evaluation of the impact of phase disturbance in a fiber cable on the transfer function of the sounder, it is also important to understand the same effect on the CIR. Even in a perfectly suppressed image signal, when $b = 0$, these phase variations could result in the distortion of the shape of CIR. The total added phase for $b = 0$, according to Eq. (5), is $\Delta\psi(f) = \phi(f) - N\theta$. The added delay observed in CIR can then be expressed as

$$\Delta\tau = -\frac{1}{2\pi} \frac{d\Delta\psi(f)}{df}. \quad (14)$$

This equation suggests that any change in the effective length of the fiber cable due to environmental disturbance manifests in the frequency-dependent phase variation $\phi(f)$ of the IF link in the cable. In contrast, the $N\theta$ term is constant across different frequencies and should therefore not contribute to any delay shift. However, if the frequency sweep duration of the VNA is considerably long and the multiply factor N is high, θ variations during a VNA sweep can appear as frequency dependent $N\theta$ in (13), possibly leading to a distortion of the CIR.

IV. EXPERIMENTS

A. Measurement Setup

Two of Aalto's channel sounders operating in the V-band and D-band RF were utilized to validate the uncertainties described in Section III. Some of the sounder parameters are listed in Table I. The VNA was set to collect 10,001 data points and use 20 KHz IF bandwidth. Furthermore, we refer to the two optical fiber links carrying the IF and LO signal as OF-IF and OF-LO, respectively.

Three conditions of the optical fiber cable were considered in the measurements and are denoted as:

- I The optical fiber cable is held in a fixed position within some duration defined in the succeeding subsections.
- II The optical fiber cable is oriented in 50 distinct positions and the frequency sweep is performed some minutes after the position is set.
- III The optical fiber cable is mounted on a rotator and is continuously dragged on the floor for 15 minutes.

The purpose of condition I is to obtain the sounder's baseline performance in the absence of any mechanical disturbance. Condition II represents the scenario during measurement campaigns, e.g., [5], with changing positions of the optical fiber cable. Condition III represents the scenario when the fiber cable is accidentally disturbed during frequency sweep or when it is continuously disturbed.

The performance of the optical fiber cable and of the sounder with varying suppression levels of image side band, b , was evaluated under different fiber cable conditions defined as I, II and III. For each set of measurements, the mean of 50 B2B measurements was used as $H_{b2b}(f)$ which is needed for calibration. In addition, instead of performing OTA measurements, only the controlled B2B measurements were conducted to assure that changes in measured transfer functions are solely due to the disturbances to the channel sounder components. Knowing that now $H_{dut}(f) = H_{att}(f)$ and using Eq. (1) and Eq. (4), $\Delta H_{cs}(f)$ was calculated by

$$\frac{H(f)}{H_{b2b}(f)} = \frac{\Delta H_{cs}(f) \cdot H_{cs}(f) \cdot H_{att}(f)}{H_{cs}(f) \cdot H_{att}} = \Delta H_{cs}(f). \quad (15)$$

A Hamming window function and IFFT were applied to $\Delta H_{cs}(f)$ to get $\Delta h_{cs}(\tau_p)$, where τ_p is the delay of the peak component. Ideally, $20 \log_{10}(\Delta|h_{cs}(\tau_p)|) = 0$ dB and $\tau_p = 0$ ns, and the rest of CIR is noise and signal leakage attributed to band limitation. However, due to disturbances to the cable, variations of $\Delta|h_{cs}(\tau_p)|$ and τ_p were observed. We report their maximum variation across each set of measurements in the next subsections. Maximum variation in τ_p is denoted here as τ_1 and the maximum variation of the peak gain is given by

$$G_i = 20 \log_{10} \frac{\Delta|h_{cs}(\tau_p)|_{max}}{\Delta|h_{cs}(\tau_p)|_{min}}, \quad (16)$$

where $\Delta|h_{cs}(\tau_p)|_{max}$ is the maximum and $\Delta|h_{cs}(\tau_p)|_{min}$ is the minimum change of the CIR magnitude in a set of measurements. The maximum variation of the gain and LO phase offset of $\Delta H_{cs}(f)$ in OF-LO measurements, denoted as G_t and θ_t , respectively, were also obtained.

The CIR distortion was further evaluated by measuring the minimum spurious-free dynamic range (SFDR) of the CIR [9]. It is the difference of the peak level and the next largest spurious peak or noise level in dB. In this paper, we define three different SFDRs such as $SFDR_{0.5}$, $SFDR_{2.5}$, and $SFDR_{5.0}$ corresponding to spurs measured at least 0.5, 2.5, and 5.0 ns away from the CIR peak, respectively.

TABLE II
MAXIMUM VARIATION OF THE CIR PEAK GAIN AND DELAY IN OF-IF
AND MINIMUM SFDR

Condition	G_i (dB)	τ_i (ns)	$SFDR_{0.5}$ (dB)	$SFDR_{2.5}$ (dB)	$SFDR_{5.0}$ (dB)
I	0.0	0.00	42.2	47.3	52.4
II	0.1	0.00	42.3	47.9	52.4
III	0.1	0.02	36.2	45.5	49.0

B. Optical Fiber Cable Measurements

The transfer functions of the two optical fiber links OF-IF and OF-LO were first measured as an individual component. In condition I, the cable was held in a fixed position and the frequency sweep was performed every 20 seconds for 12 hours in a room with a standard heater. The gain, phase and delay were found to be significantly varying for the first two hours which can be attributed to the warm-up time of the sounder components. The condition I results presented here are based on the data collected beyond this warm-up time. A summary of the OF-IF performance in various conditions is listed in Table II. All of the measured parameters have negligible variation in all the conditions which confirm the stability of OF-IF.

The phase response of the OF-LO over time under condition I at various f_{lo} values are shown in Fig. 3. The slow variation in time is most likely due to the gradual change in the room temperature. The phase fluctuations were pronounced as f_{lo} increases. The gain and phase variations of OF-LO in conditions I-III are summarized in Table III. The results from OF-IF and OF-LO measurements show that the gain does not significantly vary in all the conditions, supporting the assumption in Section III-A that optical fiber disturbance only introduces phase variations.

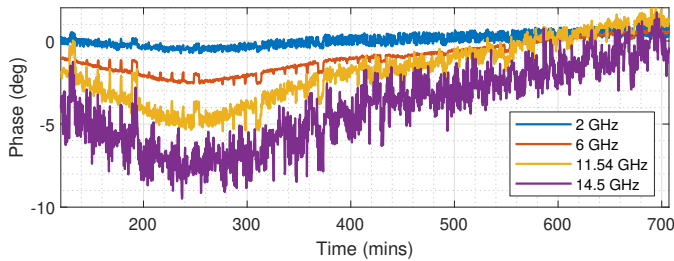


Fig. 3. OF-LO phase variation in static condition at four continuous wave frequencies.

C. Double-sideband Measurements

The sounder setup in Fig. 1 was tested for double-sideband (DSB) channels by excluding the hybrid coupler from the V-band sounder and the BPF from the D-band sounder, leading to b close to 1. The optical fiber cable was subject to condition II and two of the measured $\Delta|H_{cs}(f)|$ for D-band are plotted in Fig. 4 as solid curves. Note that the optical fiber cable is in arbitrary position and hence has likely distinct LO phase offset θ in each curve. Simulated gain plots using Eq. (13)

TABLE III
MAXIMUM VARIATION OF THE OF-LO MAGNITUDE AND PHASE IN
TRANSFER FUNCTIONS

Condition	Parameter	2 GHz	6 GHz	11.54 GHz	14.5 GHz
I	G_t (dB)	0.2	0.1	0.3	1.2
I	θ_t (deg)	1.8	3.4	7.6	11.2
II	G_t (dB)	0.1	0.1	0.3	0.3
II	θ_t (deg)	4.7	14.6	28.4	35.6
III	G_t (dB)	0.2	0.1	0.2	0.7
III	θ_t (deg)	6.8	21.7	43.9	54.2

TABLE IV
MAXIMUM VARIATION OF THE CIR PEAK GAIN AND DELAY AND
MINIMUM SFDR OF V-BAND SOUNDER

Condition -Setup	G_i (dB)	τ_i (ns)	$SFDR_{0.5}$ (dB)	$SFDR_{2.5}$ (dB)	$SFDR_{5.0}$ (dB)
I-DSB	0.1	0.00	41.4	46.0	51.8
II-DSB	4.8	0.07	23.2	40.2	45.2
III-DSB	6.5	0.37	7.6	24.1	29.0
I-SSB	0.1	0.00	41.0	46.2	50.7
II-SSB	0.5	0.00	26.0	40.7	48.1
III-SSB	0.8	0.07	16.8	25.3	29.5

are also overlaid in the figure as dashed curves. Equation (8) was linearized assuming $l = 0.15$ m, $a = 1.651$ mm and $f_{rf} = 140$ to 144 GHz, resulting in $\beta_1 = -3.1712 \times 10^{-21}$ and $\beta_0 = 1.1011 \times 10^{-9}$. The θ values were set such that the simulated plots resemble the measured plots. As predicted in Section III-B, transfer function gain changes with phase variation θ and frequency when one of the sidebands is not properly suppressed.

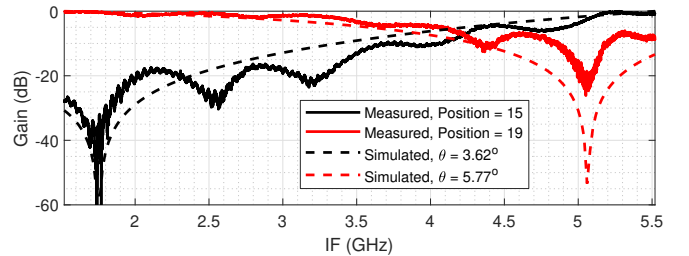


Fig. 4. Measured and simulated transfer function gain of the D-band sounder without image signal suppression ($b = 1$).

The measured CIR peak variations and their SFDR are analyzed for the DSB setup in conditions I-III, denoted by I-DSB, II-DSB and III-DSB. Results for the V-band and D-band sounders are summarized in Table IV and Table V, respectively. Significant gain and delay variations, and SFDR degradation were observed when the sounders are operated in DSB and subject to conditions II and III.

D. Single-sideband Measurements

The sounders were configured to operate in SSB channel in this set of measurements. The D-band sounder has at least 17 dB IRR, while the V-band has at least 20 dB IRR corresponding to $b = 0.14$ and $b = 0.10$, respectively. The measured $\Delta|h_{cs}(\tau)|$ of the V-band and D-band sounders when subject

TABLE V
MAXIMUM VARIATION OF THE CIR PEAK GAIN AND DELAY AND
MINIMUM SFDR OF D-BAND SOUNDER

Condition -Setup	G_i (dB)	τ_i (ns)	$SFDR_{0.5}$ (dB)	$SFDR_{2.5}$ (dB)	$SFDR_{5.0}$ (dB)
I-DSB	4.6	0.00	25.7	40.8	45.4
II-DSB	19.0	0.25	4.5	21.8	25.2
III-DSB	23.4	1.27	2.7	13.3	14.4
I-SSB	0.4	0.00	33.8	40.0	44.2
II-SSB	1.0	0.00	25.7	38.1	46.3
III-SSB	6.2	0.37	7.9	18.6	20.7

to conditions I-III are shown in Fig. 5 and Fig. 6, respectively. The results show that the peak gain is highly stable and the delay shift is unnoticeable even in condition III. Large SFDR degradation in condition III is observed due to $\phi(f)$ and $N\theta$ which both fluctuates during frequency sweep. Due to the use of Hamming window, the signal leakage attributed to band limitation does not impact the SFDR estimates. It can also be noticed that the CIR distortions for the D-band sounder are more pronounced than the V-band sounder because of the former's higher N . The CIR peak gain and delay variation,

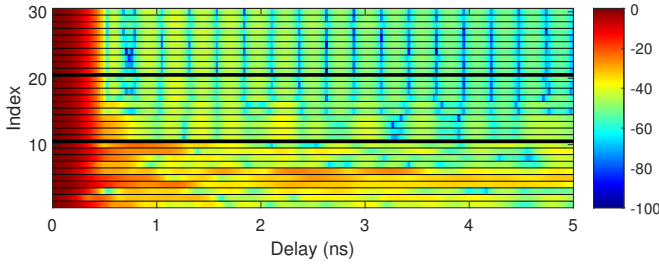


Fig. 5. CIR gain (dB) of V-band sounder operating in SSB when the optical fiber cable is subject to (top) condition I, (middle) condition II, and (bottom) condition III.

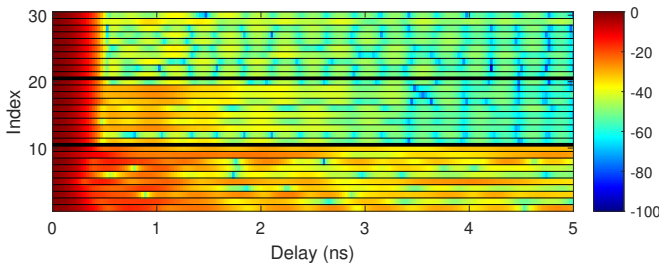


Fig. 6. CIR gain (dB) of D-band sounder operating in SSB when the optical fiber cable is subject to (top) condition I, (middle) condition II, and (bottom) condition III.

and SFDR of the SSB setup of the V-band and D-band sounders are summarized in Tables IV and V, respectively. The II-SSB setup, highlighted with the bold face in Tables IV and V, specifies the performance of Aalto's V-band and D-band sounders when performing field measurements. These results suggest that performing channel sounding in scenarios similar to conditions I and II provide reliable measurements,

while condition III may only be acceptable up to some extent due to the noticeable variation in gain, delay and SFDR.

V. CONCLUDING REMARKS

In this paper, measurement uncertainties in VNA-based sounders that utilize RoF and frequency converters such as Aalto's mm-wave sounders and other sounders, e.g. [10], were discussed. An analytical relationship of the channel sounder's transfer function with the phase variations due to the disturbance of the optical fiber cable, the limited image suppression and dispersion in the waveguide were described. These factors are shown to cause uncertainty of CIRs. Among them, the primary source of uncertainty in our case is the continuously changing physical stress on OF-LO as the resulting phase variation is magnified in the frequency converters. The uncertainty was observed as noticeable decrease of SFDR. The maximum observed CIR peak variations of Aalto's V-band and D-band sounders were 0.5 dB and 1.0 dB according to our measurements, respectively, when configured in SSB and when subject to different cable positions.

ACKNOWLEDGEMENT

This work was supported by the European Union's Horizon 2020 research and innovation programmes "Artificial Intelligence Aided D-band Network for 5G Long Term Evolution (ARIADNE)" under grant agreement #871464, "A flagship for B5G/6G vision and intelligent fabric of technology enablers connecting human, physical, and digital worlds (Hexa-X)" under grant agreement #10101596 and also by the LuxTurrin5G project funded by the participating companies and Business Finland.

The first author acknowledges the support of the Department of Science and Technology - Science Education Institute (DOST-SEI) of the Philippines for his research.

REFERENCES

- [1] C. Gentile *et al.*, "Methodology for benchmarking radio-frequency channel sounders through a system model," *IEEE Trans. Wireless Commun.*, vol. 19, no. 10, pp. 6504–6519, 2020.
- [2] G. Matz *et al.*, "On the systematic measurement errors of correlative mobile radio channel sounders," *IEEE Trans. Commun.*, vol. 50, no. 5, pp. 808–821, 2002.
- [3] R. S. Thomä *et al.*, "Identification of time-variant directional mobile radio channels," *IEEE Trans. Inst. Meas.*, vol. 49, no. 2, pp. 357–364, 2000.
- [4] K. Haneda *et al.*, "Estimating the omni-directional pathloss from directional channel sounding," in *Proc. 10th European Conf. Ant. Prop. (EuCAP 2016)*, Davos, Switzerland, Apr. 2016.
- [5] S. Nguyen *et al.*, "Comparing radio propagation channels between 28 and 140 GHz bands in a shopping hall," in *Proc. 12th European Conf. Ant. Prop. (EuCAP 2018)*, London, UK, Apr. 2018.
- [6] A. Dezfouliyan and A. M. Weiner, "Evaluation of time domain propagation measurements of uwb systems using spread spectrum channel sounding," *IEEE Transactions on Antennas and Propagation*, vol. 60, no. 10, pp. 4855–4865, 2012.
- [7] A. W. Mbugua *et al.*, "Phase-compensated optical fiber-based ultrawide-band channel sounder," *IEEE Trans. Microwave Theory Tech.*, vol. 68, no. 2, pp. 636–647, 2020.
- [8] D. M. Pozar, *Microwave Engineering, 4th Edition*. Wiley, 2011.
- [9] J. Li *et al.*, "System design and calibration for wideband channel sounding with multiple frequency bands," *IEEE Access*, vol. 5, pp. 781–793, 2017.
- [10] J. Medbo *et al.*, "60 ghz channel directional characterization using extreme size virtual antenna array," pp. 176–180, 2015.